Ducted turbine theory with right angled ducts

S McLaren-Gow[1], P Jamieson[1], J M R Graham[2]

[1] Wind Energy Systems Centre for Doctoral Training, University of Strathclyde, 204 George Street, Glasgow, G1 1XW, United Kingdom
[2] Department of Aeronautics, Imperial College London, South Kensington Campus, London, SW7 2AZ, United Kingdom

E-mail: scott.mclaren-gow@strath.ac.uk

Abstract. This paper describes the use of an inviscid approach to model a ducted turbine – also known as a diffuser augmented turbine – and a comparison of results with a particular one-dimensional theory. The aim of the investigation was to gain a better understanding of the relationship between a real duct and the ideal diffuser, which is a concept that is developed in the theory. A range of right angled ducts, which have a rim for a 90° exit angle, were modelled. As a result, the performance of right angled ducts has been characterised in inviscid flow. It was concluded that right angled ducts cannot match the performance of their associated ideal diffuser and that the optimum rotor loading for these turbines varies with the duct dimensions.

1. Introduction

Appropriate ducting around the circumference of a wind turbine rotor can augment the mass flow through that rotor and so increase the power coefficient achieved. Research on these ducted turbines – some also known as Diffuser Augmented Wind Turbines – has a long history, with many authors attempting to develop the concept and improve wind turbine performance. Notable contributions include early work by Lilley and Rainbird [1], wide ranging investigations by Foreman et al [2] and Igra [3] and the attempted development of a full scale commercial turbine by Vortec Energy [4]. Research has continued since and several small scale ducted turbines have entered production [5].

These investigations have generally taken one of three approaches to modelling a ducted turbine: one-dimensional analysis, experimentation with models in a wind tunnel and simulations with Computational Fluid Dynamics (CFD). While one-dimensional analyses can provide a more general understanding of the principles of ducted turbine performance, empirical parameters are invariably required to provide results for a particular duct. Experiments and CFD simulations do not suffer this limitation, but with the downside of much increased complexity.

This work concerns an alternative approach in which the duct and wake are modelled using a panel method. This does not require empirical parameters and is less complex than the experiment and CFD approaches. The main advantage, however, is the inviscid nature of the method. This allows the fundamental aspects of ducted turbine performance to be examined separate from the limitations imposed by viscosity. Importantly, an inviscid approach also allows for the validation of one-dimensional theory without concern for differences caused by viscous effects.

Of particular interest is the one-dimensional theory developed by Jamieson [6]. This introduces the concept of an ideal diffuser: one of infinitely variable shape to account for the changing interaction between the diffuser and a variably loaded rotor. While this concept is obviously entirely theoretical in nature, it has definite consequences for the design of real ducted turbines. Where the ideal diffuser is optimised for every rotor loading by virtue of its variable geometry, the real diffuser of fixed geometry can be optimum for only one loading. Further, each ideal diffuser has a corresponding set of real diffusers, each potentially optimised for one loading. If this concept was fully understood and the theory validated, it would provide the opportunity to maximise the performance of a real ducted turbine. In turn, this could lead to a reduced cost of wind energy.

This work concerns an investigation to determine if right angled ducts match the maximum performance of their associated ideal diffusers. This paper will begin by describing some of the background theory and the reasoning for investigating right angled ducts, give details of the modelling approach used, then present the results of the investigation.

2. Background

The ideal diffuser concept is not one that has yet been fully defined. From the theory [6], however, two things are known. First, as has been described, the ideal diffuser is of variable shape. Second, with this variable shape, the ideal diffuser provides maximum power output at a thrust coefficient of 8/9. This is the optimum balance between blockage of the flow and energy extraction; in general, real ducted turbines may have different optimum thrust coefficients if the duct is more effective at lower rotor loadings. The relationship between the performance of an ideal diffuser and an associated real diffuser is illustrated in Figure 1, as described in the theory developed by Jamieson. As can be seen, the real diffuser matches the performance of the ideal diffuser at only one value of axial induction at the rotor and hence at only one value of rotor loading. In all other situations, performance is lower. This provides a motivation for investigating this theory; an increased understanding of the ideal diffuser concept may assist in developing new principles of ducted turbine design that could maximise the performance of a real diffuser relative to an associated ideal diffuser.

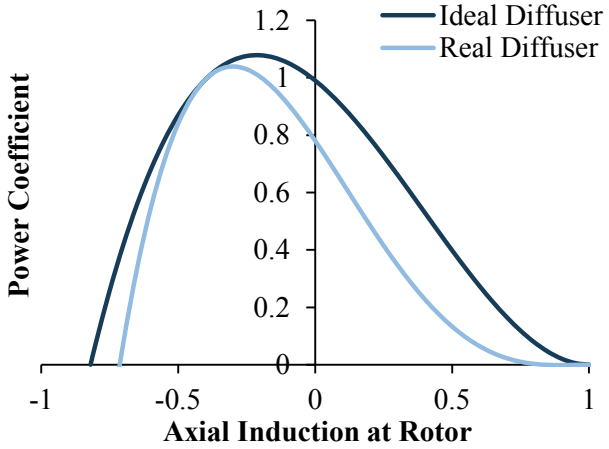

Figure 1. Qualitative illustration of ideal diffuser and real diffuser performance.

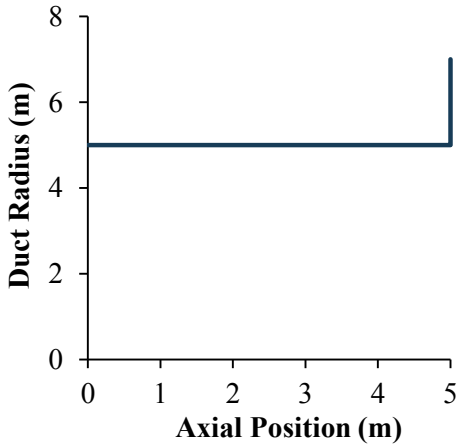

Figure 2. Shape indicated as optimum in previous study [7].

A previous investigation into this theory led to the study described in this paper. The previous work involved finding the shape which maximized mass flow rate through the rotor within certain geometrical constraints [7]. An optimisation algorithm was used to vary duct shape in two cases: $C_t = 0$ and $C_t = 8/9$. The radius of the duct was specified at three axial

positions, with a complete description of the shape provided by interpolating between these points with a cubic Hermite spline that respected monotonicity. The radius and axial position of the first and last points were fixed, which provided a constant length, inlet radius, and outlet radius for the ducts. The optimisation algorithm acted to vary the axial position and radius of the central point, with bounds formed by the axial positions and radii of the end points.

Under these restrictions, the optimisation process indicated that the best shape consisted of a sharp right angle for both loadings, as shown in Figure 2. This duct provided maximum power at $C_t = 0.79$, substantially less than 8/9, implying that this duct cannot match the maximum performance of the associated ideal diffuser. This, however, is only one possible right angled duct shape out of many; no general conclusions could be made from this single result. The study described in this paper, therefore, was undertaken to investigate the possibility that a right angled duct could provide maximum power at a thrust coefficient of 8/9. Such a discovery wouldn't necessarily lead immediately to practical benefits, as separation in real viscous flow would cause very different performance to that found in these inviscid simulations. However, showing theoretically that a ducted turbine can provide maximum power at a thrust coefficient of 8/9 or discounting the entire class of right angled shapes from the search are both useful results.

3. Model

An axisymmetric vortex panel method was employed to model the duct and turbine wake. Each duct and turbine wake panel consisted, in general, of a discrete vortex ring and a collocation point at which boundary conditions were enforced. The rotor itself was represented simply as an actuator disc generating a pressure drop that was applied uniformly across the duct cross-section; this pressure drop was an input to the simulation. The wake boundary was assumed to be a vortex tube of varying radius to satisfy the requirement of being force-free. Figure 3 and Figure 4 illustrate the constituent parts of the model.

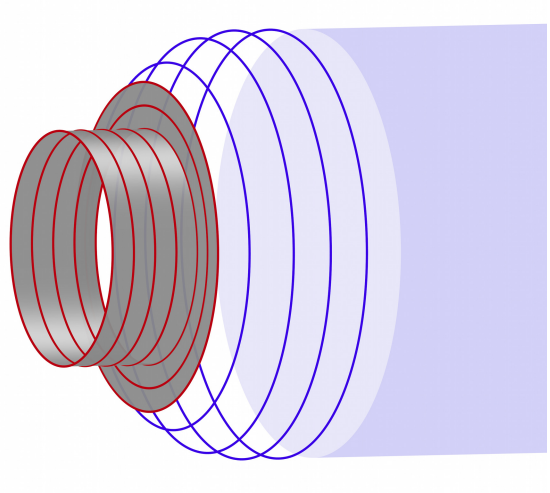

Figure 3. Qualitative illustration of model constituent parts. Shown from left to right are the duct rings, wake rings, and semi-infinite vortex cylinder. The duct shape represented by the rings is shaded.

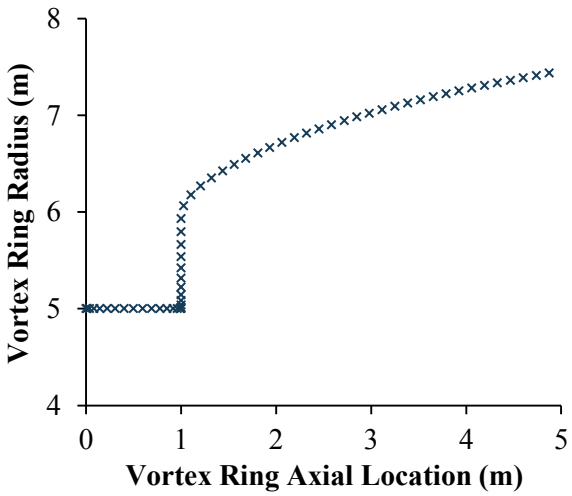

Figure 4. Location and radius of duct and wake vortex rings in an example simulation, for axial locations from 0m to 5m from duct inlet.

The solution process was iterative in nature, involving three layers of iterative calculations. For each iteration of the top layer, the middle layer was iterated until convergence; and for

each iteration of the middle layer, the bottom layer was iterated until convergence. In the top layer of iterations, the wake panels were rotated such that they remained on the wake boundary. For each top layer iteration, the middle layer found duct and wake panel strengths. A change in wake panel strengths required the recalculation of duct panel strengths and vice versa. Duct panel strengths were calculated analytically, while the bottom layer of iterations was used for each calculation of wake panel strengths.

3.1. Duct Model

The duct was modelled without thickness and was formed by a set of vortex rings unevenly distributed along its length, to provide a reduced panel length near the duct leading edge and at the right angled corner. Collocation points were placed at half the distance between each ring. A further collocation point was placed a half panel length from the last ring, marking the end of the duct. The radius of each ring and the radial position of each collocation point were set to the radius of the duct at their axial locations.

The duct vortex ring strengths were calculated on the basis of achieving zero normal flow on the duct boundary. Equation (1) expresses this, where $\boldsymbol{q}$ is the velocity vector at a point on the duct wall and $\boldsymbol{n}$ is the surface normal vector at that point. This condition was evaluated at each of the collocation points.

$$\boldsymbol{q}\cdot\boldsymbol{n} = 0 \tag{1}$$

The duct vortex strengths were solved in a two step process [8]. In the first step, coefficients were calculated that described the influence of each vortex ring on each collocation point. This coefficient is defined in equation (2), where a_{ij} is the influence coefficient of ring j on collocation point i, $\boldsymbol{U_{ij}}$ is the velocity induced at i by ring j set to unit strength and $\boldsymbol{n_i}$ is the surface normal vector at i.

$$a_{ij} = \boldsymbol{U_{ij}}\cdot\boldsymbol{n_i} \tag{2}$$

Equation (1), equation (2) and the contributions of the free stream velocity and the velocity induced by the wake vorticity can be combined into matrix notation as in equation (3), where Γ_j is the strength of ring j, $\boldsymbol{V}_\infty$ is the free stream velocity and $\boldsymbol{w_i}$ is the velocity induced by the entire wake at i. The second step of the duct solution process was to populate and solve this matrix for the vortex strengths.

$$\begin{bmatrix} a_{11} & \cdots & a_{1j} \\ \vdots & \ddots & \vdots \\ a_{i1} & \cdots & a_{ij} \end{bmatrix} \begin{bmatrix} \Gamma_1 \\ \vdots \\ \Gamma_j \end{bmatrix} = \begin{bmatrix} -\boldsymbol{V}_\infty\cdot\boldsymbol{n_1}-\boldsymbol{w_1}\cdot\boldsymbol{n_1} \\ \vdots \\ -\boldsymbol{V}_\infty\cdot\boldsymbol{n_i}-\boldsymbol{w_i}\cdot\boldsymbol{n_i} \end{bmatrix} \tag{3}$$

3.2. Wake Model

A constant panel length was used to define the wake, which was cylindrical at the start of each simulation. The vortex rings and collocation points forming the wake surface were placed at the centre of each panel, at the radius of the duct exit. The panel length was set equal to the distance between the last two duct collocation points to prevent numerical problems caused by an abrupt change in panel length. The discrete wake elements were terminated downstream by a semi-infinite vortex cylinder [9], placed at the end of the last wake panel, in order to improve accuracy and avoid the unrealistic end shape of a finite length wake. The strength per unit length of the cylinder was set equal to that of the last wake panel.

The wake vortex strengths were calculated so to prevent a pressure discontinuity across the wake. The solution process for the wake was developed from the Bernoulli equation applied twice at a collocation point on the wake surface: once for each side of the point. Equation (4) was calculated for the side outside the wake whilst equation (5) was calculated for the side

inside the wake, where ρ is the air density, P is the static pressure, ΔP is the pressure drop across the turbine, + signifies the side of the point outwith the wake and – the side in the wake.

$$\frac{1}{2}\rho|\boldsymbol{V}_\infty|^2+P_\infty = \frac{1}{2}\rho|\boldsymbol{V}_+|^2+P_+ \tag{4}$$

$$\frac{1}{2}\rho|\boldsymbol{V}_\infty|^2+P_\infty-\Delta P = \frac{1}{2}\rho|\boldsymbol{V}_-|^2+P_- \tag{5}$$

To enforce the boundary condition, the static pressures on both sides of the point were set equal, leading to equation (6).

$$\Delta P = \frac{1}{2}\rho(|\boldsymbol{V}_+|+|\boldsymbol{V}_-|)(|\boldsymbol{V}_+|-|\boldsymbol{V}_-|) \tag{6}$$

This equation can be considered in terms of the average of the velocities on the two sides of the collocation point, $\bar{\boldsymbol{V}}$, and the step change in velocity between the two sides, $\boldsymbol{\Delta V}$. The rest of the solution method assumes that these velocities are aligned; this assumption is satisfied by the converged wake shape.

The step change in velocity across the wake's vortex sheet was caused by the vorticity local to the collocation point. The approximation of a discrete vortex ring no longer sufficed in this case and a single segment of the ring immediately adjacent to the collocation point was replaced by a constant strength element. The velocity difference was therefore described by equation (7), where Δs is the length of the panel and Γ is the strength of the panel.

$$|\boldsymbol{V}_+|-|\boldsymbol{V}_-| = |\boldsymbol{\Delta V}| = \frac{\Gamma}{\Delta s} \tag{7}$$

The average velocity was then simply the velocity induced at the collocation point by the free stream, all other duct and wake rings, the vortex cylinder, and the non-singular part of the vortex ring on the panel under consideration. This is shown in equation (8), where $\boldsymbol{a}$ is the velocity induced by the remainder of the ring set at unit strength and $\boldsymbol{V}_{\mathbf{other}}$ is the velocity induced by the free stream, all other rings in the model and the vortex cylinder.

$$\frac{1}{2}(|\boldsymbol{V}_+|+|\boldsymbol{V}_-|) = \left|\bar{\boldsymbol{V}}\right| = |\boldsymbol{a}\Gamma+\boldsymbol{V}_{\mathbf{other}}| \tag{8}$$

Substituting equation (7) and (8) into equation (6) resulted in equation (9). Solving for Γ led to a quartic equation with no analytical solution. A numerical method was used instead during the solution process.

$$\Delta P = \rho|\boldsymbol{a}\Gamma+\boldsymbol{V}_{\mathbf{other}}|\frac{\Gamma}{\Delta s} \tag{9}$$

Equation (10) shows the initial estimate of the strength for all wake rings used to start iterations. This was calculated by attributing $\bar{\boldsymbol{V}}$ only to the free stream velocity. Iterations continued based on equation (9) until convergence of the ring strengths was reached.

$$\Gamma = \frac{\Delta P \Delta s}{\rho V_\infty} \tag{10}$$

3.3. Wake Shape

The wake panel positions were changed during the solution process so that they remained on the wake boundary and so that the wake could take up a converged shape satisfying the force-free condition. In the desired state each panel was aligned with the velocity local to it.

To set the wake shape, the velocity at each collocation point was first calculated, and so the desired angle of each panel found. Starting at the duct exit, each panel in turn was then rotated

around its upstream end so that it matched the calculated angle. Shape iterations continued until the shape of the wake was within a specified percentage of the last shape calculated and each panel was orientated to within a specified percentage of the local flow velocity.

3.4. Power and Thrust Calculation

The power produced by the rotor was calculated from equation (11), where A_d is the area of the rotor disc and V_d is the axial component of velocity at the disc. The velocity used was an area weighted average over the disc, calculated by finding the velocity in each of 250 annuli. Thrust was calculated using equation (12).

$$Power = \Delta P A_{\mathrm{d}} V_{\mathrm{d}} \tag{11}$$

$$Thrust = \Delta P A_{\mathrm{d}} \tag{12}$$

4. Results and discussion

All the results presented here use the standard wind turbine definitions; power and thrust coefficients, C_p and C_t, are referenced to the rotor area and free stream velocity. The rotor was placed at the duct inlet in all cases.

A convergence study was conducted to determine the required number of vortex rings, the required wake length and the required convergence criteria. Vortex rings and wake length were chosen, based on two test cases, so that a doubling of the number of rings resulted in a change in maximum power coefficient, C_{pmax}, of less than 3% and a change in thrust coefficient for maximum power, C_{topt}, of less than 1%. Simulation convergence was measured between iterations through duct and wake panel strengths, and axial and radial positions of wake panel ends. Convergence was considered reached when the maximum change in results between two iterations was 0.03% or less. The maximum difference in angle between wake panels and local flow velocity also had to be less than 0.03% of the angle between the velocity and the horizontal plane. These values were chosen as negligible variation in C_{pmax} and C_{topt} was found with increased strictness

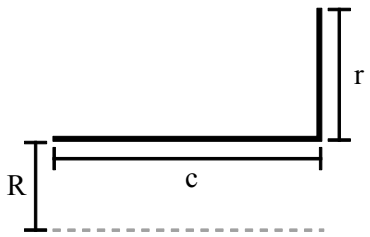

Figure 5. Definitions for duct dimensions.

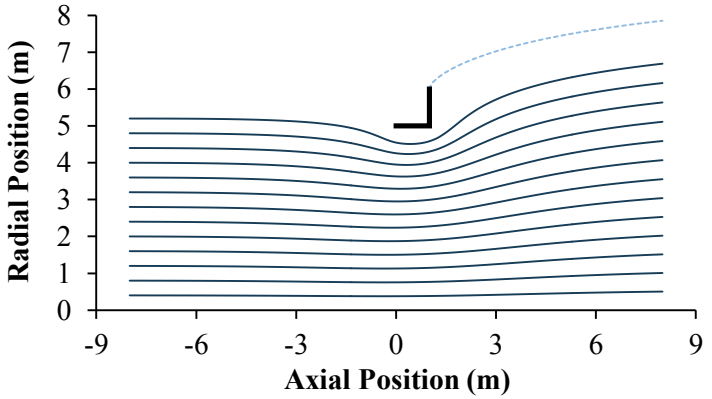

Figure 6. Streamlines of the flow through the duct with c = 1m and r = 1m at the rotor loading for maximum C_p. Flow is from left to right. Wake surface is shown by the dashed line and the rotor can be considered to be at the duct inlet.

Figure 5 illustrates the definitions used in this paper for the right angled duct dimensions. R is defined as the radius of the rotor, c is defined as the length of the duct cylindrical section, and r as the size of the radial rim. A rotor radius of 5m was used throughout this study.

Figure 6 shows streamlines for the flow passing through the duct with r = 1m and c = 1m, at the rotor loading for maximum power output, while Figure 7 shows the wake shape and panel strength. Clearly visible is a contraction of the flow as it approaches the upstream end of the duct; this demonstrates the duct acting to increase the flow velocity through the duct above the free stream value. The most substantial difference between viscous flow and the inviscid simulation results is also visible, as there is no separation seen at the duct exit. This separation would limit the performance of these right angled ducts in a way the inviscid simulations do not model.

The consequence of the lack of separation limiting performance can be seen in Figure 8, which shows the performance of all duct shapes investigated in this study; extreme values of C_{pmax} are reached. Clearly these values would not be achievable in a real flow. The results, however, are still valuable for the purposes of this study as it is the inviscid nature of the simulations that allows for a clear comparison to the theory. Further, large duct sizes are needed for a thorough investigation as there is no guarantee that the duct which provides a C_{topt} of 8/9 will be of practical dimensions.

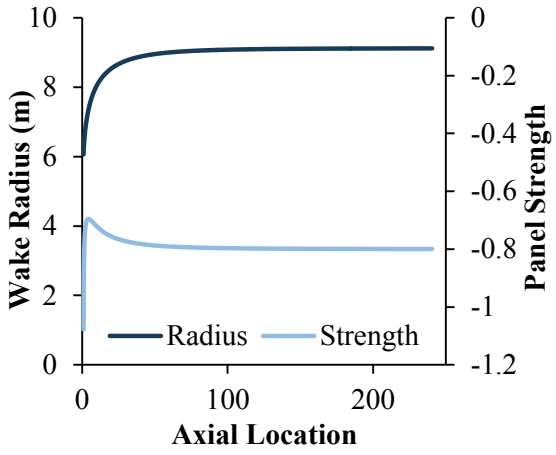

Figure 7. Radius of wake panels and their strength, for the duct with c= 1m and r = 1m at the rotor loading for maximum C_p.

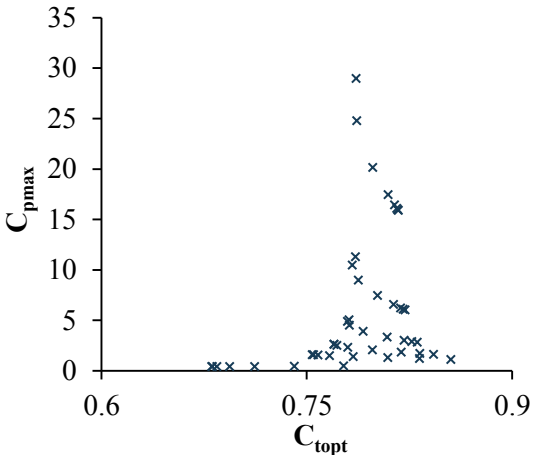

Figure 8. Plot of maximum power coefficient achieved, C_{pmax}, and the thrust coefficient to achieve it, C_{topt}, for all ducts investigated.

The first conclusion that can be drawn from Figure 8 is related to the theory; these ducts are not all associated with the same ideal diffuser. This can be established as the theory states that if they were associated with the same ideal diffuser, C_{pmax} would increase as C_{topt} approached 8/9. That is not the case here. It should be noted that many of these ducts must be associated with higher performing ideal diffusers than the one illustrated in Figure 1, as the C_{pmax} values achieved are much greater.

It is of note that C_{topt} varies with the duct dimensions, despite all the ducts being of right angled design. This is an important consideration for the design of a real ducted turbine as if the rotor is not designed for the correct loading, performance will be sub-optimal. It also can be seen in this figure that no duct was found with a C_{topt} of 8/9. The trends of C_{topt} with right angled duct design will be discussed later in this paper to determine if this is true of all right angled ducts.

Figure 9 shows C_{pmax} results for the ducts in this study, plotted against rim section size. Figure 10 shows the same results, but plotted against cylindrical section length. It can be seen that both parameters have an influence on the maximum power achieved. As cylindrical length increases, C_{pmax} appears to increase asymptotically for each rim size apart from the case where there is no rim. In this case, the cylindrical duct acts only to restrict wake expansion with no

rim section to counteract this. C_{pmax} was found to be more sensitive to rim size, with no limit to C_{pmax} found within the range of rim sizes investigated.

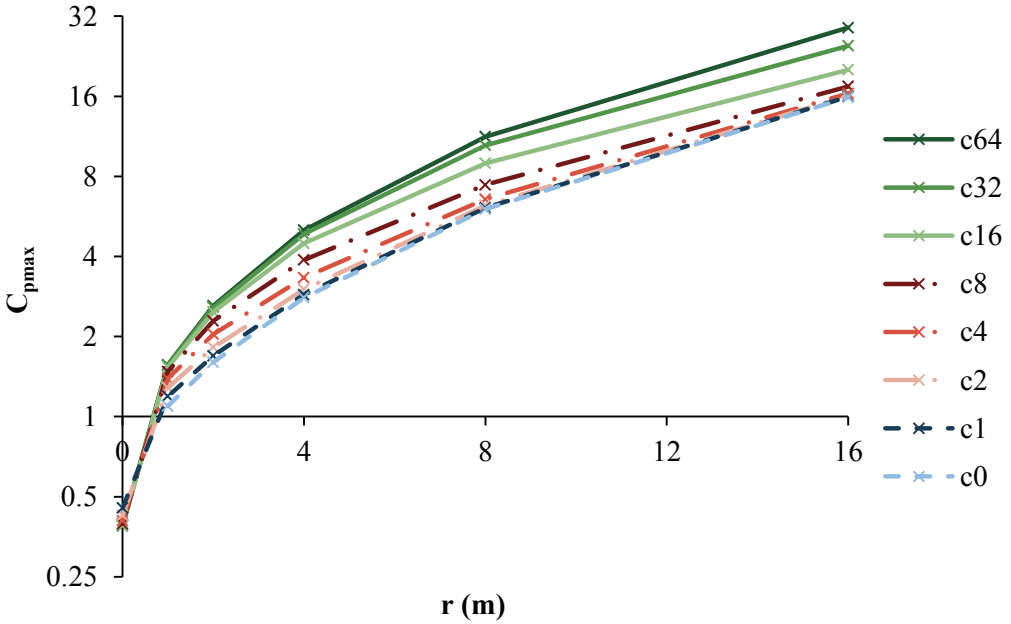

Figure 9. Variation of C_{pmax} with duct rim size, for cylindrical section lengths from 0m to 64m.

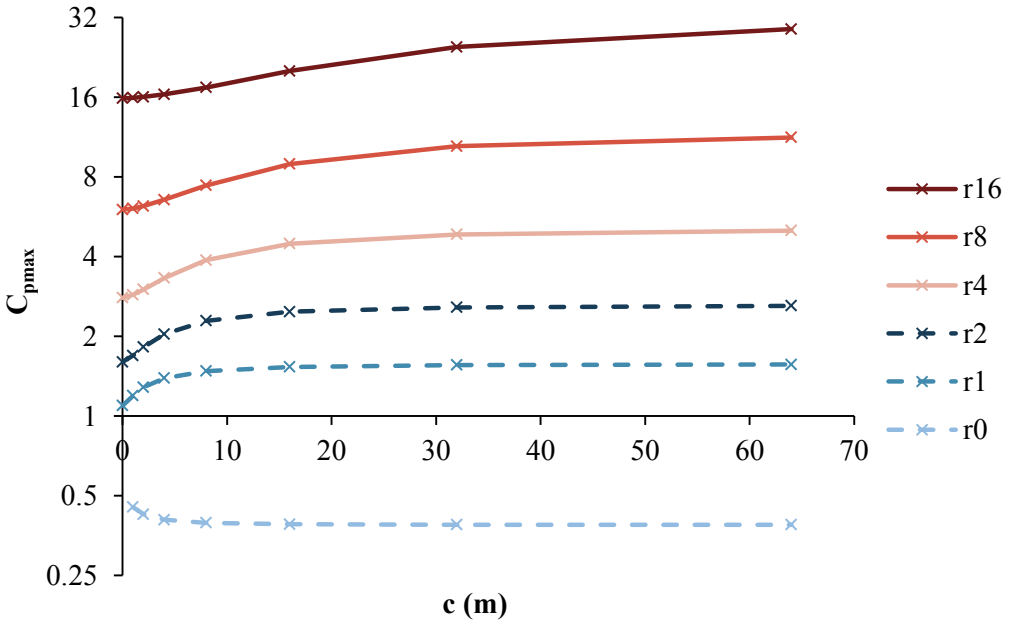

Figure 10. Variation of C_{pmax} with duct cylindrical section length, for duct rim sizes from 0m to 16m.

Figure 11 shows C_{topt} results plotted against rim size. It can be seen that the greatest variation in C_{topt} is with no rim, where the values drop away from a C_{topt} of 8/9. The only exception to this is for c = 0m, which becomes a turbine without a duct at r = 0m. As the rim

size increases, the results tend towards a smaller band of C_{topt} values around 10% lower than 8/9. It appears unlikely that increased radial size will result a C_{topt} value of 8/9.

Figure 12 shows C_{topt} results plotted against cylindrical length. With the shortest cylinders, the smallest rim size results in the largest C_{topt} values, but by c = 4m this trend has reversed and the smallest rim size results in the smallest C_{topt}. In all cases, C_{topt} decreases asymptotically with increasing cylindrical length, and it is therefore unlikely that longer cylindrical sections will lead to a C_{topt} value of 8/9.

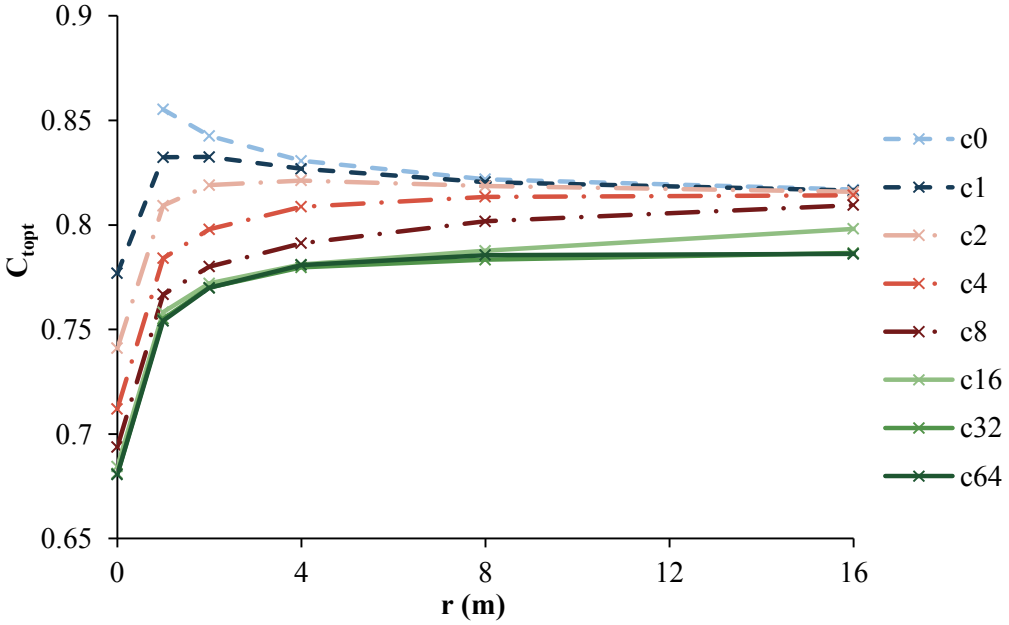

Figure 11. Variation of C_{topt} with duct rim size, for cylindrical section lengths from 0m to 64m.

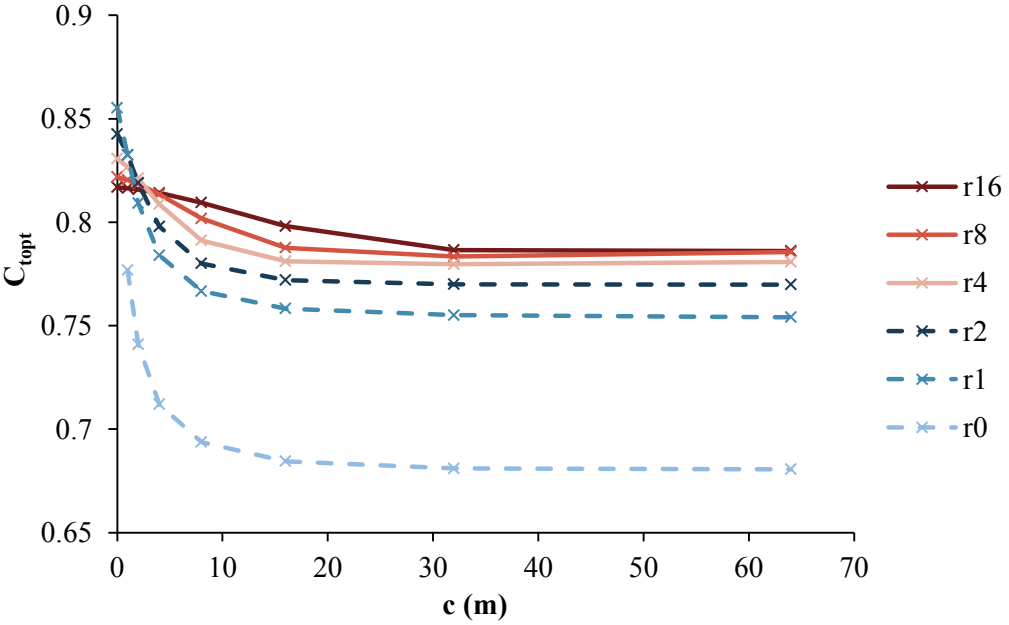

Figure 12. Variation of C_{topt} with duct cylindrical section length, for duct rim sizes from 0m to 16m.

5. Conclusions

Results have been presented for an investigation into right angled ducts, in which it was found that such ducts are not all associated with the same ideal diffuser. It can be concluded from the results presented that no right angle duct will provide maximum power output at a thrust coefficient of 8/9. From consideration of the theory, this suggests that the associated ideal diffusers are capable of greater levels of performance.

The right angled duct, however, may still be a practical design for real ducted turbines by potentially maximising performance within fixed duct size limits. At least one such turbine is under development [10]. This paper includes results which may be of use to such efforts. It has been shown that the rotor loading for maximum power varies with right angled duct dimensions; this is important for the design of a real ducted turbine as performance will be sub-optimal if the rotor does not operate at the ideal loading for the duct. Further, the performance of right angled ducts has been characterised in inviscid flow. This provides an upper bound on performance and provides a base for further study to discover how the trends in these results are affected by viscosity.

Future work will involve further comparisons to theory with the aim of increasing the levels of understanding achieved. Investigations using the described code will also be undertaken to examine the relative influence of the various parameters in duct design.

Acknowledgments

This work has been funded by the EPSRC, under project reference number EP/G037728/1.

References

[1] G. M. Lilley and W. J. Rainbird, "A Preliminary Report on the Design and Performance of Ducted Windmills," College of Aeronautics, Cranfield Report No. 102, 1956.

[2] R. A. Oman, K. M. Foreman, and B. L. Gilbert, "Investigation of Diffuser-Augmented Wind Turbines Part II - Technical Report," Grumman Aerospace Corporation, Bethpage, New York COO-2616-2(Pt.2), 1977.

[3] O. Igra, "Research and Development for Shrouded Wind Turbines," *Energy Conversion and Management,* vol. 21, pp. 13-48, 1981.

[4] R. Flay, D. Phillips, and P. Richards, "Development of Diffuser Augmented Wind Turbine Desings in New Zealand," presented at the European Wind Energy Conference, Nice, France, 1999.

[5] G. J. W. van Bussel, "The science of making more torque from wind: Diffuser experiments and theory revisited," *Journal of Physics: Conference Series,* vol. 75, p. 012010, 2007.

[6] P. Jamieson, "Generalized Limits for Energy Extraction in a Linear Constant Velocity Flow Field," *Wind Energy,* vol. 11, pp. 445-457, 2008.

[7] S. McLaren-Gow, P. Jamieson, and J. M. R. Graham, "A comparison between ducted turbine theory and inviscid simulation," in *2nd IET Renewable Power Generation Conference*, Beijing, China, 2013.

[8] J. Katz and A. Plotkin, *Low Speed Aerodynamics*, 2nd ed. Cambridge: Cambridge University Press, 2001.

[9] I. S. Gibson, "On the velocity induced by a semi-infinite vortex cylinder: with the extension to the short solenoid," *Aeronautical Journal,* vol. 78, pp. 262-268, 1974.

[10] Y. Ohya, T. Uchida, T. Karasudani, M. Hasegawa, and H. Kume, "Numerical Studies of Flow around a Wind Turbine Equipped with a Flanged-Diffuser Shroud using an Actuator-Disk Model," *Wind Engineering,* vol. 36, pp. 455-472, 2012.